Volume 210 Issue 1 February 2014 ISSN 0022-4596

ELSEVIER

JOURNAL OF SOLID STATE CHEMISTRY

IN THIS ISSUE:

A new copper borophosphate with novel polymeric chains and its structural correlation with raw materials in molten hydrated flux synthesis

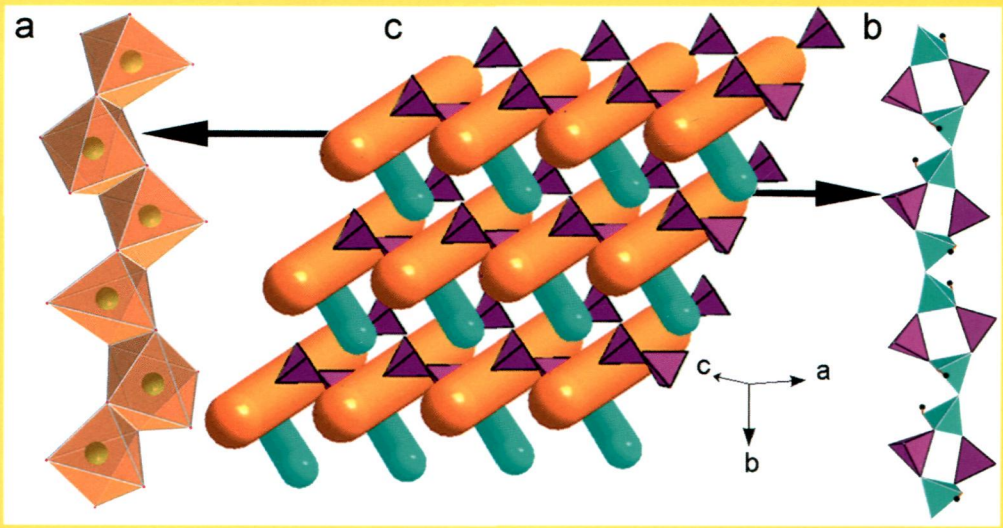

Ruijing Duan, Wei Liu, Lixin Cao, Ge Su, Hongmei Xu and Chenggong Zhao

Available online at www.sciencedirect.com

ScienceDirect

ELSEVIER

Volume 210, Issue 1, February 2014

JOURNAL OF SOLID STATE CHEMISTRY

www.elsevier.com/locate/jssc

CONTENTS

Abstracted/indexed in BioEngineering Abstracts, Chemical Abstracts, Coal Abstracts, Current Contents/Physics, Chemical, & Earth Sciences, Engineering Index, Research Alert, SCISEARCH, Science Abstracts, and Science Citation Index. Also covered in the abstract and citation database SCOPUS®. Full text available on ScienceDirect®.

Regular Articles

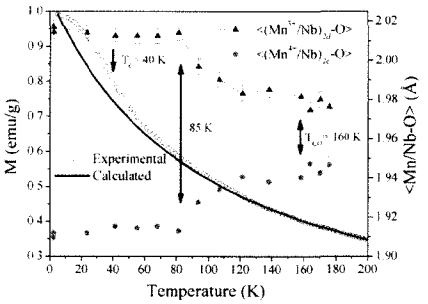

Comparison between the octahedron size and the magnetic behaviour for $Ca_3Mn_2NbO_9$ in the temperature region where the charge and magnetic order occur.

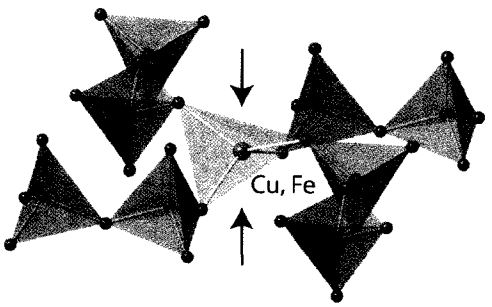

The structures of the tetragonal polymorphs of $K_2MP_2O_7$, M=Cu(II), Fe(II), consist of infinite sheets of stoichiometry $[MP_2O_7]^{2-}$, formed from linked pyrophosphate groups and MO_4 tetrahedra, separated by potassium ions. In both compounds the unusual tetrahedral coordination of the M(II) centre is strongly flattened as a result of Jahn–Teller (JT) effects for high spin, d^6 Fe(II) and p-orbital mixing and second-order JT effects for d^9 Cu(II).

Regular Articles—Continued

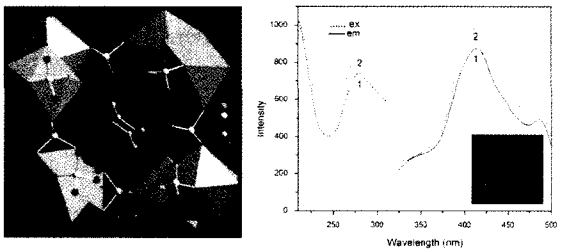

Two open-framework bismuth sulfates with the layered and three-dimensional structures have been synthesized and characterized. Both the compounds show good fluorescence properties exhibiting blue luminescence.

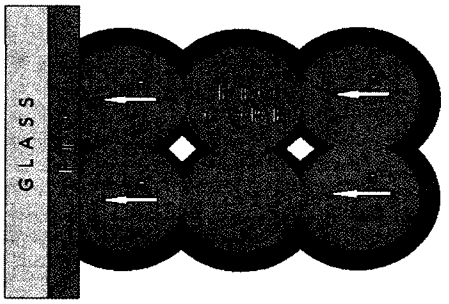

Core shell type FTO matrix was formed as TiO_2 is the shell material to create a blocking layer between FTO core and the electrolyte for suppressed recombination and efficiency enhancement.

Continued

On the peculiar properties of triangular-chain $EuCr_3(BO_3)_4$ antiferromagnet

Ł. Gondek, A. Szytuła, J. Przewoźnik, J. Żukrowski, A. Prokhorov, L. Chernush, E. Zubov, V. Dyakonov, R. Duraj and Yu. Tyvanchuk

page 30

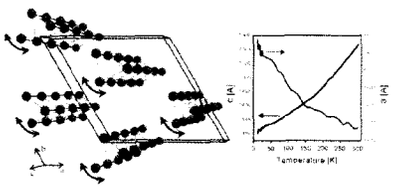

Torsion-like vibrations are the key to understand negative thermal expansion along the *a*-axis.

Syntheses, structural analyses and luminescent property of four alkaline-earth coordination polymers

Sheng Zhang, Xiao-Ni Qu, Gang Xie, Qing Wei and San-Ping Chen

page 36

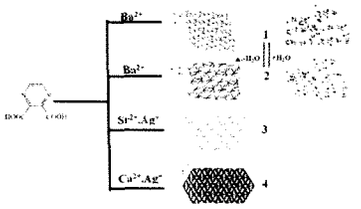

Four new coordination polymers $[Ba(Pzdc)(H_2O)]_n$ (**1**), $[Ba(Pzdc)]_n$ (**2**), $[AgSr(Pzdc)(NO_3)(H_2O)]_n$ (**3**), $[Ag_2Ca(Pzdc)_2(H_2O)]_n$ (**4**) (H_2Pzdc=2, 3-pyrazinedicarboxylic acid) have been synthesized. Compounds **1–3** display 2D topology structures and compound **4** exhibits a 3D topology structure. Fortunately, **1** and **2** undergo reversible dehydration/ rehydration of coordinated water molecules.

New tetragonal derivatives of cubic $NaZn_{13}$-type structure: RNi_6Si_6 compounds, crystal structure and magnetic ordering (R=Y, La, Ce, Sm, Gd–Yb)

M. Pani, P. Manfrinetti, A. Provino, Fang Yuan, Y. Mozharivskyj, A.V. Morozkin, A.V. Knotko, A.V. Garshev, V.O. Yapaskurt and O. Isnard

page 45

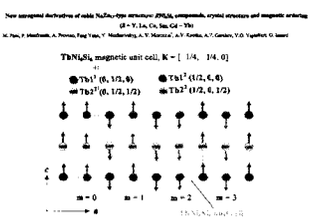

Novel {La, Ce}Ni_6Si_6 compounds adopt the new $CeNi_6Si_6$-type structure and {Y, Sm, Gd–Yb} adopt the new YNi_6Si_6-type structure that are tetragonal derivative of $NaZn_{13}$-type structure, like $LaCo_9Si_4$-type.The $CeNi_6Si_6$, $GdNi_6Si_6$, $TbNi_6Si_6$, $DyNi_6Si_6$ and $HoNi_6Si_6$ compounds are Curie–Weiss paramagnets down to ~30 K, and do not order magnetically down to 4.2 K. The powder neutron diffraction study in zero applied filed indicates square modulated the *c*-collinear antiferromagnetic ordering of $TbNi_6Si_6$ with **K**=[±1/4, ±1/4, 0] wave vector below ~10 K.

Nanocrystalline $Sm_{0.5}Sr_{0.5}CoO_{3-\delta}$ synthesized using a chelating route for use in IT-SOFC cathodes: Microstructure, surface chemistry and electrical conductivity

Rares Scurtu, Simona Somacescu, Jose Maria Calderon-Moreno, Daniela Culita, Ion Bulimestru, Nelea Popa, Aurelian Gulea and Petre Osiceanu

page 53

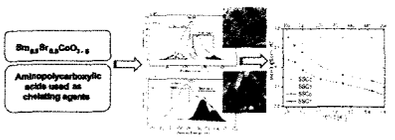

Synthesis of nanocrystalline $Sm_{0.5}Sr_{0.5}CoO_{3-\delta}$ powders by a chelating route and the investigation of the microstructure, surface chemistry and electrical properties.

A new copper borophosphate with novel polymeric chains and its structural correlation with raw materials in molten hydrated flux synthesis

Ruijing Duan, Wei Liu, Lixin Cao, Ge Su, Hongmei Xu and Chenggong Zhao

page 60

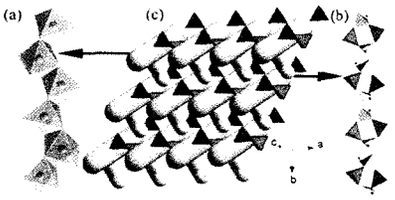

The 3D structure consists of a framework composed of CuO_x polyhedra, BO_4 and PO_4 tetrahedra. A intersection angle between the metal chains and borophosphate chains can be noted.

From $Ag_2Sb_2O_6$ to $Cd_2Sb_2O_7$: Investigations on an anion-deficient to ideal pyrochlore solid solution

Geneva Laurita, Jason Vielma, Florian Winter, Romain Berthelot, Alain Largeteau, Rainer Pöttgen, G. Schneider and M.A. Subramanian

page 65

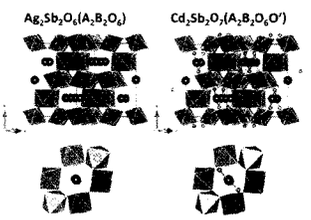

A complete solid solution between the anion-deficient pyrochlore $Ag_2Sb_2O_6$ and the ideal pyrochlore $Cd_2Sb_2O_7$ has been synthesized and investigated through various techniques including X-ray diffraction, electron paramagnetic spectroscopy, and ^{121}Sb-Mössbauer spectroscopy. Optical and electrical measurements have been performed, and computational methods have been applied to determine the density of states. Photocatalytic activity was monitored by the degradation of Methylene Blue, and upon cadmium substitution, the degradation amount decreased, which is attributed primarily to the changing optical and electrical properties of the solid solution.

Two Ce-containing 3D metal–organic frameworks: *In situ* formation of ligand (DDPD)

Xinyu Cao, Liqiong Yu and Rudan Huang

page 74

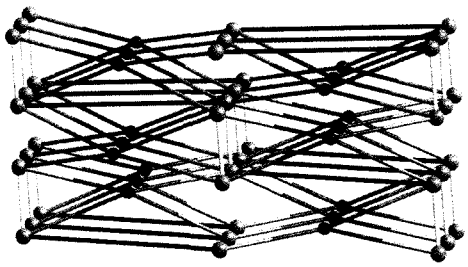

In complex **1**, the *in situ* reaction of OH-H_2BDC to DDPD(II) was found. Complex **1** features a 3D network structure. Adjacent Ce(III) ions are bridged by two carboxylate groups to form a 1D infinite inorganic chain, and further linked by the DDPD(II) ligands.

Rare-earth transition-metal gallium chalcogenides RE_3MGaCh_7 (M=Fe, Co, Ni; Ch=S, Se)

Brent W. Rudyk, Stanislav S. Stoyko, Anton O. Oliynyk and Arthur Mar

page 79

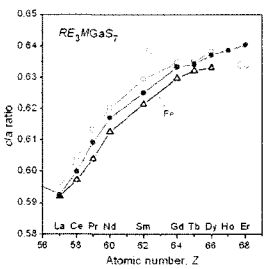

The series of chalcogenides RE_3MGaS_7, which form for a wide range of rare-earth and transition metals (M=Fe, Co, Ni), adopt highly anisotropic structures containing chains of M-centred octahedra and stacks of Ga-centred tetrahedra.

The layered antimonides $RELi_3Sb_2$ (RE=Ce–Nd, Sm, Gd–Ho). Filled derivatives of the $CaAl_2Si_2$ structure type

Marion C. Schäfer, Nian-Tzu Suen, Michaella Raglione and Svilen Bobev

page 89

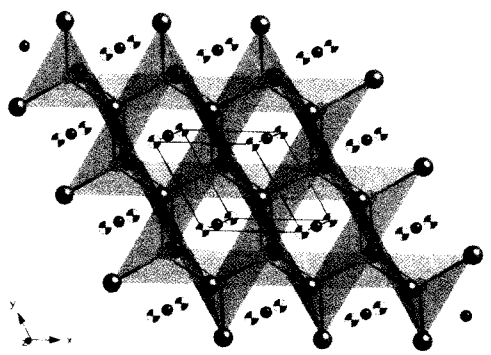

The large family of rare-earth metal–lithium–antimonides with the formula $RELi_3Sb_2$ (RE=Ce–Nd, Sm, Gd–Ho) crystallize in the trigonal space group $P\bar{3}m1$ (No. 164, Pearson symbol $hP6$) with a structure that is a filled derivative of the $CaAl_2Si_2$ structure type (ternary variant of α-La_2O_3).

Synthesis, crystal structure and magnetic properties of $Li_{0.44}Eu_3[B_3N_6]$

I. Kokal, U. Aydemir, Yu. Prots, T. Förster, J. Sichelschmidt, M. Yahyaoglu, G. Auffermann, W. Schnelle, F. Schappacher, R. Pöttgen and M. Somer

page 96

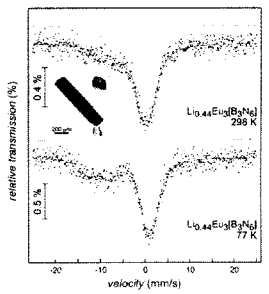

Single crystals of $Li_{0.44}Eu_3[B_3N_6]$ was obtained from the metathesis reaction of $Li_3[BN_2]$ and $EuCl_3$. ^{151}Eu Mössbauer, ESR and magnetic susceptibility measurements reveal the heterogeneous mixed valency of the Eu atoms.

Phase equilibria in the quasi-ternary system Ag_2Se–Ga_2Se_3–In_2Se_3 and physical properties of $(Ga_{0.6}In_{0.4})_2Se_3$, $(Ga_{0.594}In_{0.396}Er_{0.01})_2Se_3$ single crystals

I.A. Ivashchenko, I.V. Danyliuk, I.D. Olekseyuk and V.V. Halyan

page 102

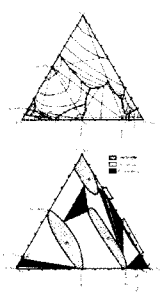

The article reports for the first time the investigated liquidus surface projection of the Ag_2Se–Ga_2Se_3–In_2Se_3 system and isothermal section at 820 K of the system. Five phase diagrams, six polythermal sections, isothermal section at 820 K and the liquidus surface projection were built at the first time. The existence of the large region of the solid solutions based on $AgIn_5Se_8$, Ga_2Se_3 and $AgGa_{1-x}In_xSe_2$ was investigated. The existence of two ternary phases was established in the Ga_2Se_3–In_2Se_3 system. Two single crystals $(Ga_{0.6}In_{0.4})_2Se_3$, $(Ga_{0.594}In_{0.396}Er_{0.01})_2Se_3$ were grown and some of optical properties of them were studied at first time.

Continued

Synthesis of layered double hydroxide nanosheets by coprecipitation using a T-type microchannel reactor

Xiujiang Pang, Meiyu Sun, Xiuming Ma and Wanguo Hou

page 111

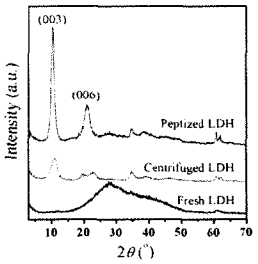

Layered double hydroxide (LDH) nanosheets were synthesized by coprecipitation using a T-type microchannel reactor, and could be used as basic building blocks for LDH-based functional materials.

Fabrication and temperature-dependent magnetic properties of one-dimensional multilayer Au–Ni–Au–Ni–Au nanowires

S. Ishrat, K. Maaz, Kyu-Joon Lee, Myung-Hwa Jung and Gil-Ho Kim

page 116

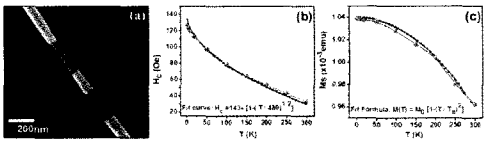

(a) SEM image of Au–Ni–Au–Ni–Au nanowire with 230 nm Ni segment length and 180 nm Au sandwiched between Ni segments (b) Kneller's law (c) Bloch's law

---

One-pot synthesis of a metal–organic framework as an anode for Li-ion batteries with improved capacity and cycling stability

Lei Gou, Li-Min Hao, Yong-Xin Shi, Shou-Long Ma, Xiao-Yong Fan, Lei Xu, Dong-Lin Li and Kang Wang

page 121

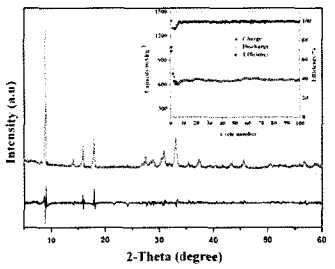

The PXRD pattern and the cycleability curves (inset) of $Co_2(OH)_2BDC$.

Homochiral Cu(II) and Ni(II) malates with tunable structural features

Marina S. Zavakhina, Denis G. Samsonenko, Alexander V. Virovets, Danil N. Dybtsev and Vladimir P. Fedin

page 125

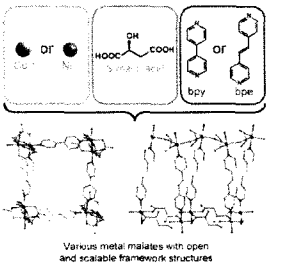

Four new homochiral metal–organic frameworks are built from Ni^{2+} or Cu^{2+} cations, *S*-malate anions and N-donor linkers of different length, which controls the size of pores and guest accessible volume of the homochiral structure.

One-step synthesis of layered yttrium hydroxides in immiscible liquid–liquid systems: Intercalation of sterically-bulky hydrophobic organic anions and doping of europium ions

Mebae Watanabe and Shinobu Fujihara

page 130

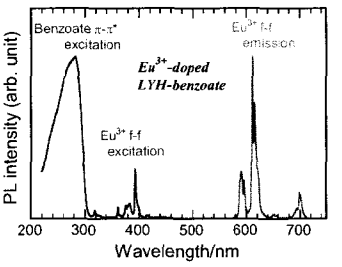

The Eu^{3+}-doped layered yttrium hydroxide exhibits intense red photoluminescence after intercalation of benzoate ions.

Template synthesis and luminescence properties of TiO_2:Eu^{3+} nanotubes

Huan Zhao, Keyan Zheng, Ye Sheng, Hongbo Li, Hongguang Zhang, Xiaofei Qi, Zhan Shi and Haifeng Zou

page 138

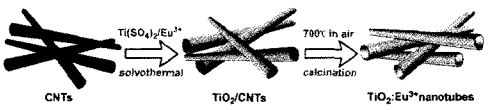

This picture is the illustration for the formation process of TiO_2:Eu^{3+} nanotubes.

Structure analysis of a Mn-doped willemite-type compound, $H_{0.12}(Zn_{1.89(3)}Mn_{0.05(1)}\square_{0.06})Si_{1.00(1)}O_4$

David Behal, Benedikt Röska, Ulf Gattermann, Alexander Reul and So-Hyun Park

page 144

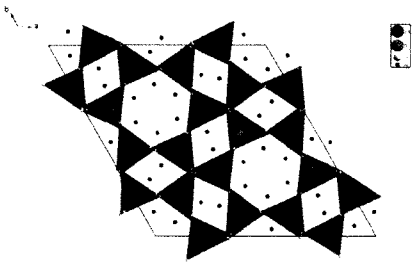

A willemite-type compound, $H_{0.12}(Zn_{1.89(3)}Mn_{0.05(1)}\square_{0.06})Si_{1.00(1)}O_4$ exhibits protons near to oxygens in the skirt of four- and six-membered ring channels, as a result of defects at two crystallographically different Zn sites.

The pressure-induced phase transition studies of In_2S_3 and In_2S_3:Ce nanoparticles

Binbin Yao, Hongyang Zhu, Shuangming Wang, Pan Wang and Mingzhe Zhang

page 150

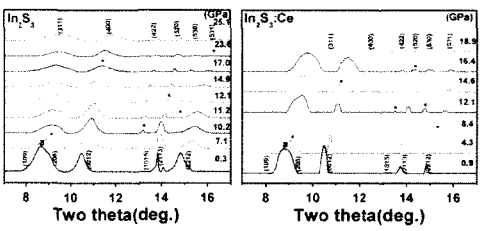

The phase transition of the In_2S_3 and In_2S_3:Ce nanoparticles have been investigated for the first time by *in situ* high pressure synchrotron X-ray in a diamond anvil cell.

New high-pressure polymorph of In_2S_3 with defect Th_3P_4-type structure

Xiaojing Lai, Feng Zhu, Ye Wu, Rong Huang, Xiang Wu, Qian Zhang, Ke Yang and Shan Qin

page 155

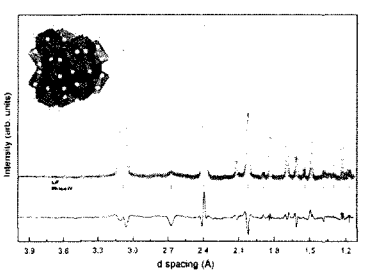

The structure and Rietveld refinement of new polymorph the defect Th_3P_4-type In_2S_3. This structure was observed at 35.6 GPa after laser heating by X-ray diffraction.

Preparation and surface modification of hierarchical nanosheets-based ZnO microstructures for dye-sensitized solar cells

Yongming Meng, Yu Lin, Yibing Lin and Jiyuan Yang

page 160

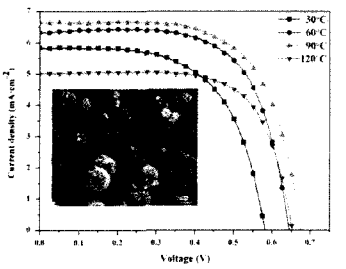

Influences on energy conversion efficiency of the dye-sensitized solar cells assembled by decorating hierarchical nanosheets-based ZnO microstructures with tetrabutyl titanate solution at different temperatures.

Synthesis and characterization of a 1D chain-like Cu_6 substituted sandwich-type phosphotungstate with pendant dinuclear Cu–azido complexes

Yan-Ying Li, Jun-Wei Zhao, Qi Wei, Bai-Feng Yang and Guo-Yu Yang

page 166

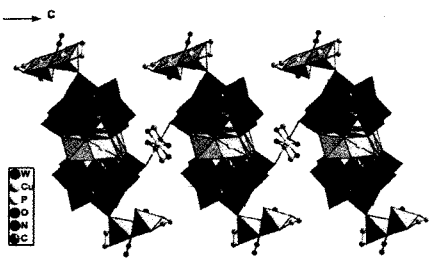

The first hexa-Cu^{II} sandwiched phosphotungstate with supporting Cu–azido complexes has been prepared and characterized.

TiO_2 synthesized by microwave assisted solvothermal method: Experimental and theoretical evaluation

K.F. Moura, J. Maul, A.R. Albuquerque, G.P. Casali, E. Longo, D. Keyson, A.G. Souza, J.R. Sambrano and I.M.G. Santos

page 171

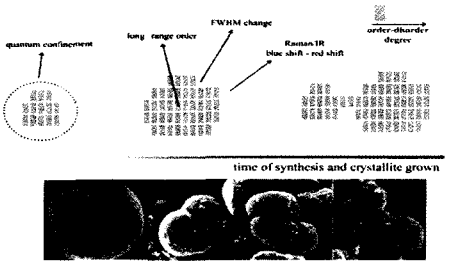

FE-SEM images of anatase obtained with different periods of synthesis associated with the order–disorder degree.

Continued

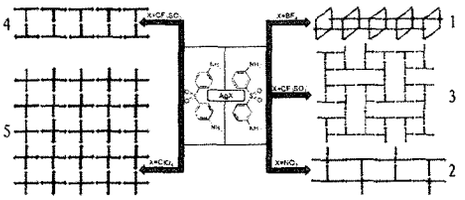

Pictogram: Synthetic procedures of the five anion controlled silver coordination polymers. We reported the synthetic procedures, structure, and luminescence property of the five anion controlled silver coordination polymers based on two novel di(aminophenyl)sulfone V-shaped ligands.

Illustration of the $A_4O_4TiSe_4$ crystal structure ($C2/m$ symmetry), A_4O and A_3TiO edge sharing tetrahedral ribbons in red, chains of edge-sharing $TiSe_4O_2$ in blue. Rare earth=green, titanium=blue, seleniu-m=yellow, and oxygen=red.

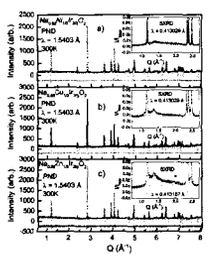

Diffraction patterns of $Na_{0.92}Ni_{1/3}Ir_{2/3}O_2$, $Na_{0.86}Cu_{1/3}Ir_{2/3}O_2$ and $Na_{0.89}Zn_{1/3}Ir_{2/3}O_2$: neutron diffraction patterns in the main panel and synchrotron diffraction in the insets. The patterns show a small amount of ordering in the transition metal iridium layer.

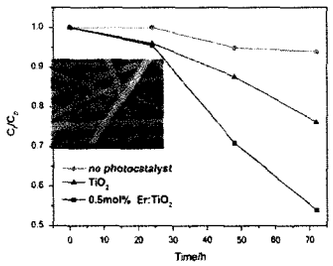

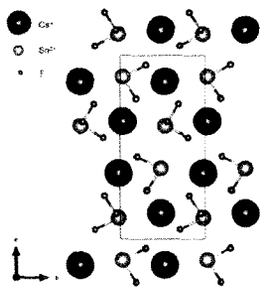

Ball-and-stick diagrams of $CsSnF_3$.

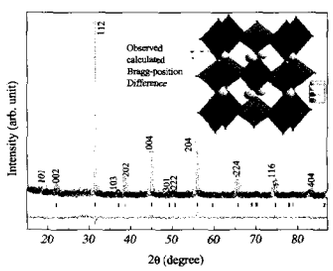

Rietveld refinement plot for BPCN. Inset shows the schematic presentation of the BPCN tetragonal unit cell. The Co^{2+} atoms are located at the centers of the CoO_6 (blue) octahedra. The Nb^{5+} atoms are located at the centers of the NbO_6 (green) octahedra.

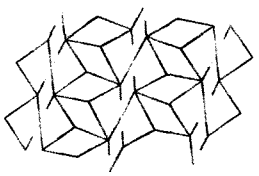

3D Sandwiched Heterometallic Framework with 3,4,5-connected Net

Two new K^+/Cu(II) and Zn(II) coordination polymers with pyridine-2,3-dicarboxylate (pydc), $\{K_2[Cu(\mu\text{-pydc})_2]\cdot 3H_2O\}_n$ (**1**) and $\{[Zn(\mu\text{-pydc})(H_2O)(4\text{-mim})]\cdot H_2O\}_n$ (**2**) (4-mim=4-methylimidazole) have been synthesized from zerovalent metal and characterized by IR, EPR spectroscopy, thermal analysis and single crystal X-ray diffraction techniques. The water soluble $\{K_2[Cu(\mu\text{-pydc})_2]\cdot 3H_2O\}_n$ shows three dimensional a rare 3,4,5-connected network with the point symbol of $\{4^2.6\}_2\{4^2.8^4\}\{4^3.6.8^6\}_2$. The temperature dependent magnetic property of complex **1** has been studied. Complex **2** exhibits unusual yellow luminescence in the solid state at room temperature.

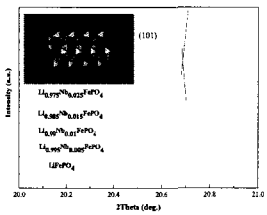

The proper amount of Nb doping widens the one dimensional diffusion channels of Li^+ along the [0 1 0] direction.

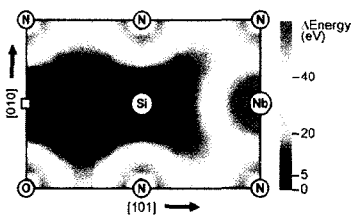

Potential energy scan of the Si atom in the most stable $Si_3\square O_3N$ cube around the vacancy in our preliminary simulation on niobium silicon oxynitride $(Nb_{0.87}Si_{0.09}\square_{0.04})(N_{0.87}O_{0.13})$. A possible distortion of the Si atom was suggested from its octahedral towards tetrahedral position forming the local structure similar to that in amorphous SiO_2.

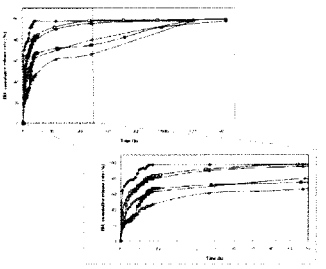

Ibuprofen release profiles for the materials obtained from samples P84_meso (black diamonds), P84_20% (white squares), P84_50% (black triangles), P84_75% (white diamonds), P84_75% functionalized by grafting (black squares) and P84_75% functionalized by co-condensation method (white triangles).

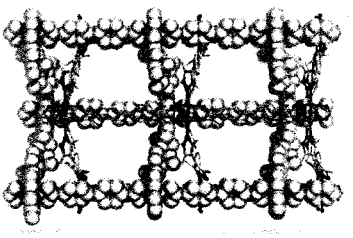

A new pillared-layer porous framework has been constructed by paddle-wheel $Co_2(O_2C\text{-}R)_4$ cluster and H_2bpdc–H_2bpz mixed ligands, displaying adsorption selectivity and antiferromagnetic properties.

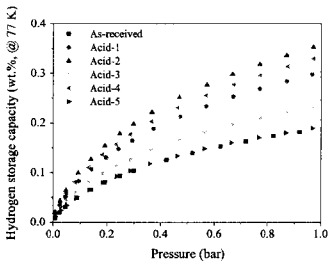

Hydrogen storage behaviors of the *p*-type MWNTs with the acid-mixed treatments are described.

Continued

2D→3D polycatenated and 3D→3D interpenetrated metal–organic frameworks constructed from thiophene-2,5-dicarboxylate and rigid bis(imidazole) ligands

Hakan Erer, Okan Zafer Yeşilel, Mürsel Arıcı, Seda Keskin and Orhan Büyükgüngör

page 261

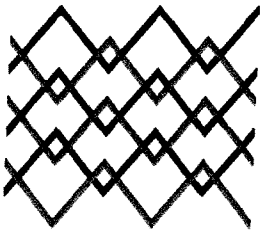

In this study, hydrothermal reactions of rigid 1,4-bis(imidazol-1-yl) benzene (dib) and 1,4-bis(imidazol-1-yl)-2,5-dimethylbenzene (dimb) with deprotonated thiophene-2,5-dicarboxylic acid (H_2tdc) in the presence of Zn(II) and Cd(II) salts in H_2O produced three new metal–organic frameworks. Isomorphous complexes **1** and **2** reveal polycatenated 2D+2D→3D framework based on an undulated (4,4)-sql layer. Complex **3** exhibits a new 4-fold interpenetrating 3D framework with the point symbol of 6^6. Molecular simulations were used to assess the potentials of the complexes for H_2 storage application. These coordination polymers exhibit blue fluorescent emission bands in the solid state at room temperature.

Substitution studies of Mn and Fe in $Ln_6W_4Al_{43}$ (Ln=Gd, Yb) and the structure of $Yb_6Ti_4Al_{43}$

LaRico J. Treadwell, Pilanda Watkins-Curry, Jacob D. McAlpin, Joseph Prestigiacomo, Shane Stadler and Julia Y. Chan

page 267

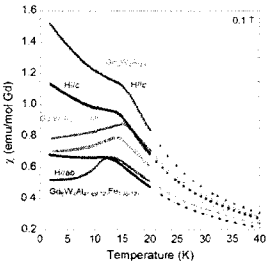

The magnetic susceptibility of $Ln_6W_{4-x}Al_{43-y}T_{x+y}$ (Ln = Gd, Yb; T= Mn, Fe).

Ferroelectric performances and crystal structures of (Pb, La)(Zr, Ti, Nb)O_3

Naoto Kitamura, Takuma Mizoguchi, Takanori Itoh and Yasushi Idemoto

page 275

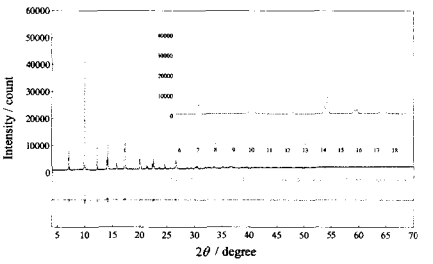

Rietveld refinement pattern of 2 mol% $PbSiO_3$-added $Pb_{0.95}La_{0.05}Zr_{0.50}Ti_{0.45}Nb_{0.05}O_3$ (synchrotron X-ray diffraction).

Gas adsorption/separation properties of metal directed self-assembly of two coordination polymers with 5-nitroisophthalate

Mürsel Arıcı, Okan Zafer Yeşilel, Seda Keskin and Onur Şahin

page 280

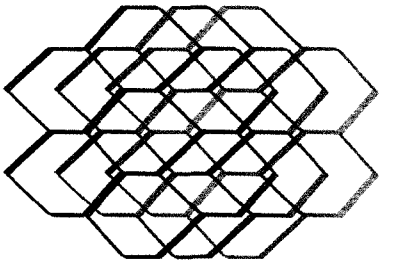

In this study, two new coordination polymers, namely, $[Co(\mu\text{-nip})(\mu\text{-bpe})]_n$ (**1**) and $[Zn(\mu\text{-nip})(\mu\text{-bpe})]_n$ (**2**) (nip: 5-nitroisophthalate, bpe: 1,2-bis(4-pyridyl)ethane) were hydrothermally synthesized and structurally characterized by single crystal X-ray diffraction, IR spectroscopy, elemental analysis and thermal analysis. Moreover, atomically detailed simulation studies of complex **2** for CO_2/CH_4 adsorption and separation were performed. Complex **1** consists of two dimensional (2D) (4,4) grid networks with the point symbol of $4^4.6^2$. Complex **2** exhibits a 3-fold interpenetrating 3D framework with $6^5.8$-dmp topology. Simulation studies demonstrated that complex **2** can separate CO_2 from CH_4 at low pressures at 273 K.